Preparation and Crystal Structures of Manganese, Iron, and Cobalt Complexes of the Bis[di(2-pyridyl)methyl]amine (bdpma) Ligand and Its Oxidative Degradation Product 1,3,3-Tris(2-pyridyl)-3*H*-imidazo[1,5-*a*]-pyridin-4-ium (tpip); Origin of the bdpma Fragility

Catherine Hemmert, Michael Renz, Heinz Gornitzka, Stéphanie Soulet, and Bernard Meunier*[a]

Abstract: The synthesis and structural characterization of manganese, iron, and cobalt complexes of bis[di(2-pyridyl)-methyl]amine (bdpma) were investigated. The bdpma ligand can give rise to mono- or dimeric complexes. Moreover, bdpma can undergo oxidative degradation leading to 1,3,3-tris(2-pyridyl)-3*H*-imidazo[1,5-*a*]pyridin-4-ium (tpip) or to starting materials used for the preparation of bdpma. During attempts to prepare manganese, iron, or cobalt complexes of the tpip ligand, two classes of compounds were obtained. The first class corresponded to the tpip cation with a simple exchange of counterion and the second class led to a new type of complex, which involved a modification of tpip and contained the *N*-(di(2-pyridyl)methoxymethyl)(di(2-pyridyl)imine) (dpmmdpi) ligand. This work has allowed us to understand the fragility of the bdpma ligand, which is due to the easily activated benzylic C–H bonds in the α position to the heteroatom.

Keywords: cobalt · iron · manganese · N ligands · oxidative degradation

Introduction

Catechol dioxygenases, a class of nonheme iron enzymes, are implicated in important metabolic reactions of environmental relevance.[1] This class of enzymes catalyzes the oxidative cleavage of intra- or extradiol C–C bonds of various catechols using molecular oxygen.[1] Several synthetic functional models have been described. Among these, iron(III) complexes [Fe(L)(dbc)], where L is a tetradentate, tripodal ligand (for example L = *N*,*N*′-dimethyl-2,11-diaza[3.3](2,6)pyridinophane[2] or tris[(2-pypyridyl)methyl]amine;[3] dbc = 3,5-di-*tert*-butylcatecholate dianion) react with dioxygen to afford oxidative cleavage of dbc, mimicking the intradiol cleavage of catechol dioxygenases. Funabiki et al. recently reported that 3- and 4-chlorocatechols that contain an electron-withdrawing substituent can also be oxidatively cleaved with molecular oxygen, using a nonheme iron(III) complex.[4]

In our group, we recently observed the oxidative degradation of different catechols using hydrogen peroxide and cobalt or iron tetrasulfophthalocyanine complexes (CoPcS or FePcS).[5] The latter complex has also been used in the oxidative degradation of 2,4,6-trichlorophenol (TCP), a major pollutant in the chlorine bleaching of wood pulp.[6] The catalytic oxidation of the poorly biodegradable catechol or TCP substrates led not only to the corresponding benzoquinones but also to ring cleavage products.[5, 6] However, little is known about the potential use of nonheme mononuclear complexes in the catalytic oxidation of such pollutants. In order to investigate the activity of this category of catalysts, we decided to prepare a new polypyridine ligand and to determine the capacity of its iron or manganese complexes as catalysts in TCP degradation (for a recent report on the catalytic activity of an iron tetrapyridyl complex in alkane oxidation, see ref. [7]).

We recently reported the synthesis of the new symmetric polypyridine ligand bis[di(2-pyridyl)methyl]amine (bdpma, Scheme 1).[8] The bdpma ligand was designed in analogy to the *N*,*N*-bis(2-pyridylmethyl)-*N*-bis(2-pyridyl)methylamine (N4Py) ligand.[7] bdpma was synthesized in a one-pot, two-step reaction consisting of refluxing di(2-pyridyl)methylamine (**A**) and di(2-pyridyl)ketone (**B**) in isopropanol in the presence of molecular sieves and acetic acid, and subsequent reduction with zinc dust (Scheme 1). The main advantages of this synthesis are the good yield (70%) and the ability to obtain bdpma in large amounts without using hazardous reagents or potentially explosive materials (like perchlorate salts).[8] The coordination of pentadentate bdpma to transition

[a] Dr. B. Meunier, Dr. C. Hemmert, Dr. M. Renz, Dr. H. Gornitzka, S. Soulet
Laboratoire de Chimie de Coordination du CNRS
205 route de Narbonne, F-31077 Toulouse cedex 4 (France)
Fax: (+33) 5-61-55-30-03
E-mail: bmeunier@lcc-toulouse.fr

  0947-6539/99/0506-1766 $ 17.50+.50/0

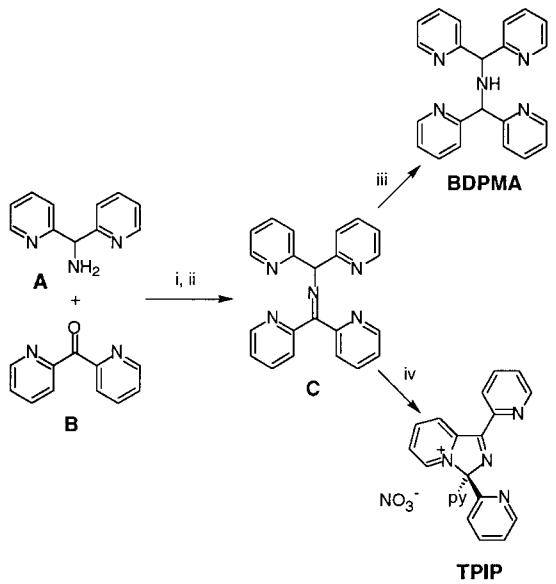

Scheme 1. Synthesis of bis[di(2-pyridyl)methyl]amine (bdpma) and 1,3,3-tris(2-pyridyl)-3*H*-imidazo[1,5-*a*]pyridin-4-ium (tpip) via the imine **C**. Reagents and conditions: i) molecular sieves 3 Å, 1 h; ii) AcOH, reflux, 5–6 h; iii) Zn; iv) MnO_2.

metals should leave one site free (in an octahedral geometry) for catalytic oxidation activity. We thus compared the catalytic activity of the mononuclear iron(III) complex $[Fe^{III}(bdpma)](NO_3)_3$ with macrocyclic complexes in the oxidation of pollutants.[9] This complex catalyzed the oxidative degradation of polychlorophenols in the presence of potassium monopersulfate as oxidant. Unfortunately, the oxidation stopped at the quinone level without the formation of ring cleavage products, and the catalyst was degraded after a few catalytic cycles (22–27).[9]

Here we report the synthesis and structural characterization of manganese, iron, and cobalt complexes of bdpma. In our efforts to crystallize these different compounds we discovered the versatile behavior of the bdpma ligand, which gives rise to mono- or dimeric complexes. Moreover, the bdpma ligand can also undergo oxidative degradation to form the cationic species 1,3,3-tris-(2-pyridyl)-3*H*-imidazo[1,5-*a*]pyridin-4-ium (tpip; for the structure see Scheme 1)[10] or, after hydrolysis, di-(2-pyridyl)ketone (**B**), one of the starting materials used for the preparation of BDMPA. Finally, we evaluated the ability of tpip to act as a ligand, using manganese, iron, and cobalt salts. This work allowed us to understand the low catalytic activity of the $[Fe^{III}(bdpma)](NO_3)_3$ complex and to discuss the origin of the fragility of the bdpma ligand.

Abstract in French: *Nous avons synthétisé et caractérisé par diffraction aux rayons X des complexes de manganèse, fer et cobalt utilisant le ligand bis[di(2-pyridyl)methyl]amine (bdpma). Des complexes de type monomère et dimère ont été respectivement isolés avec le manganèse et le fer. bdpma peut également subir, en présence d'acides de Lewis, une dégradation par oxydation conduisant soit au ligand cationique 1,3,3-tris(2-pyridyl)-3H-imidazo[1,5-a]pyridin-4-ium (tpip), soit aux précurseurs utilisés pour la préparation de bdpma. Des essais de complexation du ligand tpip par le manganèse, le fer ou le cobalt ont conduit à deux catégories de composés. La première correspond au cation tpip avec un simple échange de contreion. La seconde est représentée par un nouveau complexe qui implique une modification du composé tpip conduisant au ligand N-(di(2-pyridyl)méthoxyméthyl)(di(2-pyridyl)imine) (dpmmdpi). L'étude détaillée des différents complexes et composés obtenus nous a permis de mettre en évidence la fragilité du ligand bdpma, liée à une activation des liaisons benzyliques C–H situées en position α de l'atome d'azote de l'amine secondaire.*

Results

Complexes containing the intact bdpma ligand. X-ray structures and characterizations of $[Mn^{II}(bdpma)Cl_2]$ (1) and $[Fe^{III}_2(bdpma)_2(O)Cl_2]Cl_2(MeOH)_2$ (2): Three different transition metals (manganese, iron, and cobalt) were used in the present study, but only two complexes containing the intact bdpma ligand were observed. Complex **1** was obtained on mixing methanolic solutions of $MnCl_2$ and bdpma, followed by crystallization in a methyl *tert*-butyl ether atmosphere. By the same method, under a nitrogen atmosphere, an Fe^{III} μ-oxo dimer (complex **2**) was isolated when starting from $FeCl_2$ and bdpma. The complexes $[Mn^{II}(bdpma)Cl_2]$ (**1**) and $[Fe^{III}_2(bdpma)_2(O)Cl_2]Cl_2(MeOH)_2$ (**2**) are depicted in Scheme 2. Selected bond lengths and angles of complexes **1** and **2** are listed in Tables 1 and 2, respectively. The arrangement of the BDMPA ligand around the metal centers is similar in both complexes.

The crystal structure of complex **1** consists of a mononuclear, neutral $[Mn^{II}(bdpma)Cl_2]$ entity in a distorted octahe-

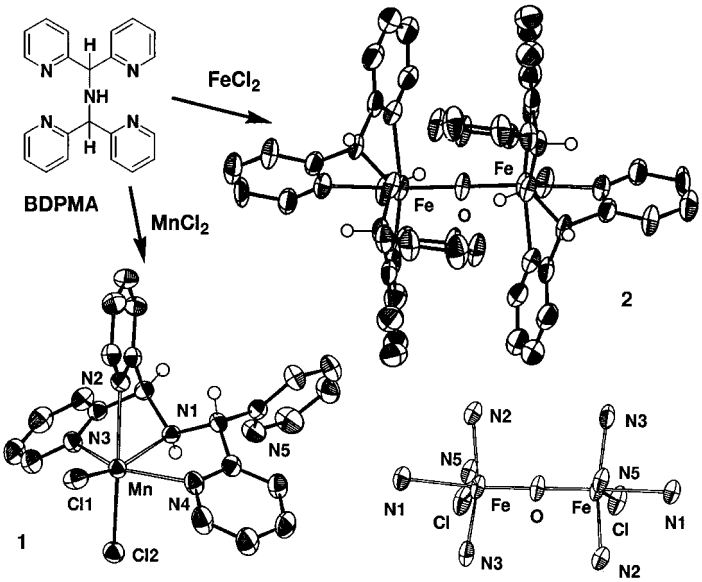

Scheme 2. Complexes containing the intact bdpma ligand: X-ray structures of $[Mn^{II}(bdpma)Cl_2]$ (**1**) and $[Fe^{III}_2(bdpma)_2(O)Cl_2]Cl_2(MeOH)_2$ (**2**) (in the latter structure, two chlorides and the two methanol molecules have been omitted for clarity).

Table 1. Selected bond lengths [Å] and angles [°] for $[Mn^{II}(bdpma)Cl_2]$ (**1**).

Mn – N(1)	2.326(2)	Mn – N(4)	2.279(2)
Mn – N(2)	2.348(2)	Mn – Cl(1)	2.413(1)
Mn – N(3)	2.337(3)	Mn – Cl(2)	2.432(1)
N(4)-Mn-N(1)	72.03(8)	N(3)-Mn-Cl(1)	118.19(6)
N(4)-Mn-N(3)	143.39(9)	N(2)-Mn-Cl(1)	91.62(6)
N(1)-Mn-N(3)	72.09(8)	N(4)-Mn-Cl(2)	90.28(7)
N(4)-Mn-N(2)	95.54(9)	N(1)-Mn-Cl(2)	98.37(7)
N(1)-Mn-N(2)	70.38(9)	N(3)-Mn-Cl(2)	87.87(7)
N(3)-Mn-N(2)	79.12(8)	N(2)-Mn-Cl(2)	164.86(7)
N(4)-Mn-Cl(1)	98.01(7)	Cl(1)-Mn-Cl(2)	101.41(6)
N(1)-Mn-Cl(1)	157.90(7)		

Table 2. Selected bond lengths [Å] and angles [°] for $[Fe_2^{III}(bdpma)_2(O)Cl_2]Cl_2\ (MeOH)_2$ (**2**).

Fe(1) – N(1)	2.323(5)	Fe(1) – N(5)	2.203(5)
Fe(1) – N(2)	2.163(5)	Fe(1) – Cl(1)	2.284(2)
Fe(1) – N(3)	2.148(6)	Fe(1) – O(1)	1.782(1)
Fe ··· Fe	3.563		
O(1)-Fe(1)-N(3)	97.34(14)	N(2)-Fe(1)-Cl(1)	100.89(15)
O(1)-Fe(1)-N(2)	94.68(14)	N(5)-Fe(1)-Cl(1)	161.80(13)
N(3)-Fe(1)-N(2)	151.7(2)	O(1)-Fe(1)-N(1)	167.0(2)
O(1)-Fe(1)-N(5)	95.4(2)	N(3)-Fe(1)-N(1)	82.66(18)
N(3)-Fe(1)-N(5)	77.5(2)	N(2)-Fe(1)-N(1)	80.00(19)
N(2)-Fe(1)-N(5)	75.9(2)	N(5)-Fe(1)-N(1)	71.83(18)
O(1)-Fe(1)-Cl(1)	102.7(2)	Cl(1)-Fe(1)-N(1)	89.98(14)
N(3)-Fe(1)-Cl(1)	101.30(16)	Fe(1)-O(1)-Fe(2)	178.6(4)

dral geometry. The square plane is formed by three nitrogen donor atoms of bdpma, two pyridine nitrogens arising from each di-(2-pyridyl)methyl moiety and the secondary amine nitrogen, and a chloride. The equatorial Mn – N bond lengths are typical, ranging from 2.279(2) to 2.337(3) Å. The axial positions, occupied by another pyridine nitrogen of the bdpma ligand and a second chloride, have longer bonds, as expected (Mn – N2 = 2.348(2) and Mn – Cl2 = 2.432(1) Å).

The crystal structure of complex **2** exhibits a (μ-oxo)-diiron(III) core with two lattice chloride anions and two methanol molecules. The metal centers are arranged in an approximate octahedral geometry. Each iron atom is coordinated to four nitrogen donor atoms of bdpma (three pyridines and the secondary amine), the bridging oxygen atom, and one chloride. The μ-oxo bridge was expected to have a strong *trans* influence towards the weakest nitrogen donor atom of bdpma, as in related complexes containing ligands with both pyridyl and amine functions.[11] However, complex **2** shows a symmetric structure in which the secondary amines of both bdpma ligands are in a *cis* position with respect to the μ-oxo bridge, with an $Fe-N_{amine}$ distance of 2.203(5) Å, and are *cis* to each other. The (μ-oxo)-diiron(III) complex of tris(2-pyridylmethyl)amine (TPA), $[Fe_2^{III}(TPA)_2(O)Cl_2]^{2+}$ reported by Toftlund et al.,[12] also contains such a symmetrical arrangement, with the two tertiary amines of both TPA ligands located *cis* to the μ-oxo bridge (and *trans* to each other).

In both complexes, steric constraints are involved and strong stacking interactions between the pyridine rings situated on each side of the μ-oxo bridge are predominant. The $Fe-N_{pyridine}$ bond *trans* to the μ-oxo bridge is longer (Fe1 – N1: 2.323(5) Å) than the $Fe-N_{pyridine}$ bonds *cis* to the bridge (mean value: 2.156 Å). The sixth coordination sites of both iron centers are occupied by terminal chloride ligands at an unusually short Fe – Cl distance of 2.284(2) Å. The chlorides are orientated *cis* to each other and *trans* to the secondary amines. The Fe – O and Fe ··· Fe distances of 1.782(1) and 3.563 Å respectively and the Fe – O – Fe angle of 178.6(4)° are typical values for linear (μ-oxo)-diiron(III) core structures.[11]

The Mössbauer spectrum of **2** recorded at 80 K consisted of a single quadrupole doublet with an isomer shift $\delta = 0.46$ mm/s (relative to metallic iron at room temperature), characteristic of two high-spin ferric centers. The quadrupole splitting, $\Delta Eq = 1.37\ mm\,s^{-1}$, is small when compared to those generally observed (in the range $1.5-2.0\ mm\,s^{-1}$) for oxo-bridged dinuclear complexes.[13] Susceptibility data for complex **2** were recorded from 300 to 5 K, under a magnetic field of 5 T. At 300 K, $\chi_M T$ is equal to $0.81\ cm^3\,K\,mol^{-1}$. This value was below that expected for two noninteracting Fe^{III} ions having g values of 2.0 ($8.75\ cm^3\,K\,mol^{-1}$). When the temperature was lowered, $\chi_M T$ decreased to a value of $0.17\ cm^3\,K\,mol^{-1}$ at 5 K. This behavior is indicative of an antiferromagnetic interaction between the two Fe^{III} ions. The experimental results obtained from 5 to 300 K can be analyzed based on a spin Hamiltonian for isotropic exchange $H = -JS_{Fe}\cdot S_{Fe}$. The experimental data were fitted to the corresponding expression[14] for two high-spin Fe^{III} local spins ($S = 5/2$), corrected for an uncoupled impurity. The best fit yielded an interaction parameter J of $-245\ cm^{-1}$, $g = 2$, $z = 0.045$ (assuming that the impurity was a high-spin Fe^{III} species; this was confirmed by the powdered EPR spectrum which showed a signal of low intensity centered at $g = 4.34$) with an agreement factor R equal to 8×10^{-4}, $R = \Sigma(\chi_{obs}T - \chi_{calcd}T)^2/\Sigma(\chi_{obs}T)^2$. All the previously reported Fe – O – Fe complexes display rather similar magnetic properties with J values in the range -170 to $-230\ cm^{-1}$.[13, 15]

The UV-visible spectrum of complex **2** did not show the characteristic band (between 550 and 700 nm, blue-shifted to a nearly 180° angle for Fe – O – Fe) of an oxo to Fe^{III} charge-transfer transition,[16] strongly suggesting that the dimer core is not maintained in solution. This is supported by IR measurements. The solid-state IR spectrum of **2** exhibited an asymmetric Fe – O stretching vibration at $840\ cm^{-1}$, which was not present in solution.

Compounds obtained by oxidative degradation of BDMPA in the presence of a transition metal salt. X-ray structure and characterization of {[Co^{III}(dpkH)$_2$](MeO)(MeOH)} (3): During attempts to crystallize a mononuclear iron(III) complex involving the bdpma ligand and $Fe(NO_3)_3$, a modified bdpma ligand was obtained instead of the expected metal complex, namely 1,3,3-tris(2-pyridyl)-3*H*-imidazo[1,5-*a*]pyridin-4-ium, [tpip](NO_3) (Scheme 3); see ref. [10] for a preliminary communication on this structure). Selected bond lengths and angles of [tpip](NO_3) are given in Table 3. The tpip cation contains an imidazopyridinium entity, in which the positively charged nitrogen (N2) is common to both the six- and five-membered rings. The C7 – N1 bond of the five-membered ring has a short length of 1.293(5) Å, consistent with a double bond conjugated to the pyridinium moiety through C6 – C7 and to the pyridine attached to C7. This is supported by the fact that

0947-6539/99/0506-1768 $ 17.50+.50/0 *Chem. Eur. J.* **1999**, *5*, No. 6

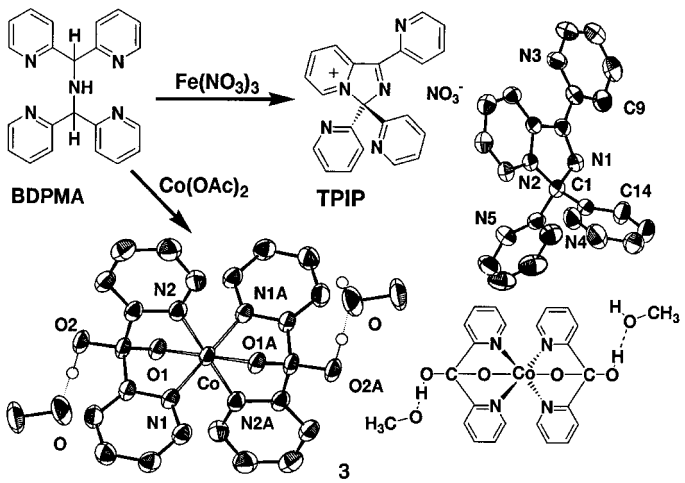

Scheme 3. Compounds obtained by the oxidative degradation of bdpma in the presence of a transition metal salt: X-ray structures of [tpip](NO_3) and [Co^{III}(dpkH)]$_2$(MeO)(MeOH) (**3**).

Table 3. Selected bond lengths [Å] and angles [°] for [tpip](NO_3), [tpip]$_2$[$Mn^{II}Cl_4$] (**4**), [tpip][$Fe^{III}Cl_4$] (**5**), and [tpip]$_2$[$Co^{II}Cl_4$] (**6**).

	[tpip](NO_3)	[tpip]$_2$[$MnCl_4$]	[tpip][$FeCl_4$]	[tpip]$_2$[$CoCl_4$]
M(1)–Cl(1)	–	2.347(2)	2.171(3)	2.280(1)
M(1)–Cl(2)	–	2.366(1)	2.191(8)	2.272(1)
C(1)–N(1)	1.457(4)	1.460(5)	1.447(4)	1.462(4)
C(1)–N(2)	1.498(4)	1.488(6)	1.284(5)	1.498(3)
C(2)–N(2)	1.336(4)	1.335(6)	1.346(4)	1.344(4)
C(2)–C(3)	1.374(5)	1.372(7)	1.371(5)	1.373(4)
C(3)–C(4)	1.383(6)	1.387(7)	1.374(5)	1.377(4)
C(4)–C(5)	1.388(5)	1.389(7)	1.389(5)	1.391(4)
C(5)–C(6)	1.377(5)	1.368(7)	1.371(5)	1.378(4)
C(6)–C(7)	1.471(5)	1.475(6)	1.483(5)	1.477(4)
C(7)–N(1)	1.293(5)	1.289(6)	1.284(5)	1.284(4)
N(1)-C(7)-C(6)	112.2(3)	112.3(4)	111.7(3)	112.5(2)
N(1)-C(7)-C(8)	121.9(3)	123.4(4)	122.9(3)	122.6(3)
N(1)-C(1)-N(2)	103.5(3)	103.7(3)	103.6(3)	103.5(2)
N(1)-C(1)-C(13)	111.3(3)	112.3(4)	111.1(3)	111.5(2)
N(1)-C(1)-C(18)	109.0(3)	109.4(3)	109.1(3)	109.8(2)
N(2)-C(1)-C(18)	109.6(3)	112.2(3)	112.1(3)	111.2(2)
N(2)-C(6)-C(5)	119.4(3)	119.3(4)	120.5(3)	119.5(3)
N(2)-C(6)-C(7)	105.2(3)	104.6(4)	105.2(3)	105.0(2)
N(2)-C(2)-C(3)	119.0(4)	118.8(4)	118.3(3)	118.4(3)
C(6)-N(2)-C(1)	109.4(3)	109.4(3)	109.4(3)	109.4(2)
C(2)-N(2)-C(1)	127.2(3)	128.0(4)	128.2(3)	127.6(2)
C(2)-N(2)-C(6)	123.1(3)	122.6(4)	122.5(3)	123.0(2)
C(7)-N(1)-C(1)	109.6(3)	110.0(3)	110.2(3)	109.6(2)

the pyridine plane containing N3 has a mean deviation of only 5° from the plane formed by the imidazopyridinium moiety. The C2–N2 bond length of 1.344(4) Å is similar to those observed in the pyridine rings (mean value: 1.340(4) Å), while the C6–N2 bond is longer, with a distance of 1.368(4) Å.

Even less of the original bdpma structure remained when this ligand reacted with $Co(OAc)_2$. Indeed, the crystal structure of the resulting complex **3**, which is depicted in Scheme 3, showed a cobalt(III) complex with two hydrates of ketone **B**. Relevant bond lengths and angles are given in Table 4. The geometry of the cationic complex {[Co^{III}(dpkH)$_2$](MeO)(MeOH)} (**3**) is almost octahedral, as would be expected for a Co^{III} species, with two di-(2-pyridyl)ketone hydrate (dpkH) moieties coordinated in a

Table 4. Selected bond lengths [Å] and angles [°] for {[Co^{III}(dpkH)]$_2$-(MeO)(MeOH)} (**3**).

Co–N(1)	1.911(3)		
Co–N(2)	1.915(3)		
Co–O(1)	1.886(2)		
O(1A)-Co-O(1)	180	O(1)-Co-N(2)	83.42(11)
O(1A)-Co-N(1)	97.19(11)	N(1)-Co-N(2)	88.75(12)
O(1)-Co-N(1)	82.81(11)	N(1A)-Co-N(2)	91.25(12)
N(1)-Co-N(1A)	180	N(2)-Co-N(2A)	180
O(1A)-Co-N(2)	96.58(11)		

tridentate mode. The dpkH ligand stabilizes the high oxidation state of the metal center better than bdpma (with four pyridine ligands), owing to the presence of the σ-donor oxygen atom.

Two negative charges to neutralize the Co^{III} center were provided by deprotonation of one hydroxy group of each ketone hydrate. The crystal structure of **3** also displays one methanolate anion, which provides the third negative charge, and one methanol molecule, which are exchangeable by symmetry. The structure depicted in Scheme 3 represents one motif of the unit cell. In addition, two lattice-disordered ethyl acetate molecules are present. The metal–ligand bond lengths are unusual because the axial Co–O1 distance of 1.886(2) Å is shorter than the equatorial (Co–N1: 1.911(3) and Co–N2: 1.915(3) Å) distances. The three angles O1–Co–O1A, N1–Co–N1A, and N2–Co–N2A are exactly 180°. The angle made by the off-axis coordination of the oxygen atom with the line normal to the equatorial plane is very small, with a value of 7.19°. Several characterization results, including the FAB mass spectrum, the ^{1}H NMR spectrum, and the absence of a magnetic susceptibility as determined by the Faraday method, support the low-spin, +3 oxidation state of the cobalt center. Moreover, the X-ray structure of the same complex has already been described by Sommerer et al.,[17] starting from [$Co(NH_3)_4CO_3$]NO_3 and two equivalents of di-(2-pyridyl)ketone in water. In this case, the counterion was a nitrate and the substantiating evidence for a Co^{III} was obtained from INDO geometry optimization calculations.[17]

Compounds obtained with tpip as a potential ligand. X-ray structures and characterizations of [tpip]$_2$[$Co^{II}Cl_4$] (6), [Fe^{II}(dpmmdpi)Cl_2] (7), and [Co_2^{II}(dpmm)$_2Cl_4$] (8): tpip was prepared in a gram scale in order to study its behavior as a potential ligand. It was efficiently synthesized from the imine **C** by oxidation with MnO_2 (Scheme 1; for the reaction mechanism see the Discussion section). During attempts to prepare tpip complexes using manganese, iron, or cobalt salts, we obtained two different categories of compounds (Scheme 4). The first category was obtained with $MnCl_2$, $FeCl_3$, and $CoCl_2$. In these cases, we were unable to get any complexation reaction and we observed [tpip][$Fe^{III}Cl_4$] (**5**), formed by the exchange of the initial anion (NO_3^-) by [$Fe^{III}Cl_4$]$^-$, when using $FeCl_3$. $MnCl_2$ and $CoCl_2$ gave doubly negatively charged [$M^{II}Cl_4$]$^{2-}$ complexes and crystallized with two molecules of tpip ([tpip]$_2$[$Mn^{II}Cl_4$] (**4**) and [tpip]$_2$[$Co^{II}Cl_4$] (**6**), respectively). The crystal structure of [tpip]$_2$[$Co^{II}Cl_4$] (**6**), which illustrated this first class of compounds, is depicted in

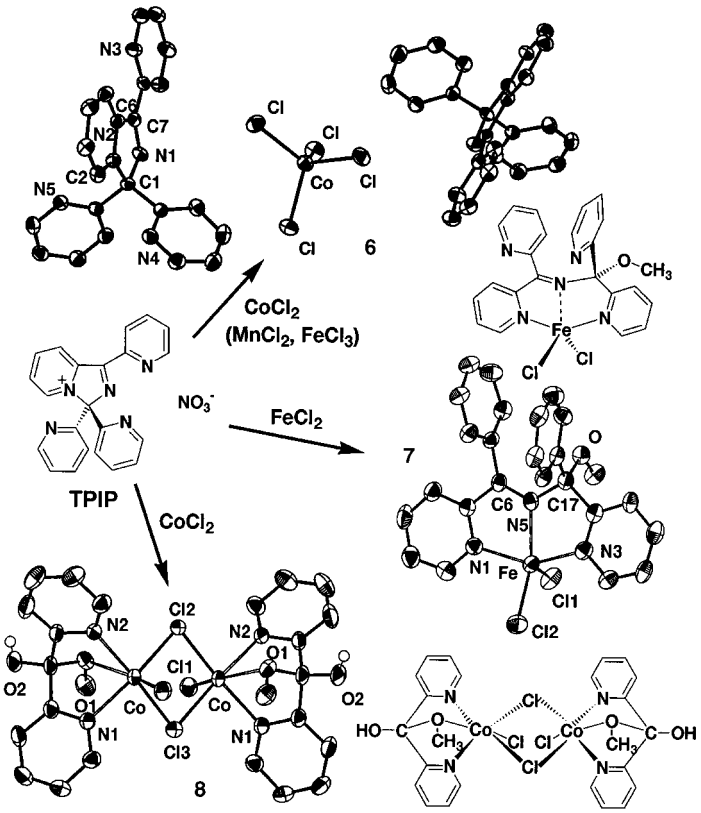

Scheme 4. Compounds obtained with tpip as potential ligand: X-ray structures of $[Co^{II}Cl_4][tpip]_2$ (**6**), $[Fe^{II}(dpmmdpi)Cl_2]$ (**7**), and $[Co^{II}_2(dpmm)_2Cl_4]$ (**8**).

Scheme 4. Selected bond lengths and angles of compound **6** are listed in Table 3. The crystal structure of the ion pair **6** consists of two cationic tpip ligands arranged around a tetrahedral tetrachlorocobaltate dianion.

In contrast to the unsuccessful complexation reactions discussed above, a new type of complex (**7**) was synthesized when tpip and $FeCl_2$ were used as starting materials. In this case, we obtained a metal complex for the first time, namely $[Fe^{II}(dpmmdpi)Cl_2]$ (**7**; dpmmdpi = *N*-(di(2-pyridyl)methoxymethyl)(di(2-pyridyl)imine)), which involves a modification of tpip (Scheme 4). The crystal structure of complex **7** is shown in Scheme 4, and selected bond lengths and angles are given in Table 5. In the structure, the dpmmdpi ligand exhibits a bdpma-like skeleton with four pyridine groups. A solvent molecule, methanol, has been incorporated into the initial tpip and the imidazole ring has been opened (ligand **E** of Scheme 5 in the Discussion section). The iron atom is in a distorted square pyramidal environment, in which the square plane is formed by one imine N5 and two pyridine (N1 and N3) nitrogens and the chloride anion Cl1. The equatorial Fe–N bond lengths range from 2.133(5) to 2.147(5) Å. The second chloride Cl2 occupies the axial position with a longer bond of 2.325(2) Å. The major difference between the dpmmdpi and bdpma ligands is the presence of an imine function linking the dipyridyl entities of dpmmdpi. The corresponding short bond length C6–N5 of 1.306(8) Å in complex **7** is in good agreement with a carbon–nitrogen double bond. In contrast, the single $C–N_{amine}$ bond of the bdpma ligand (C17–N1: 1.467(9) Å) is slightly longer in complex **2**. Another important feature of the dpmmdpi ligand is the presence of a methoxy group at the C17 carbon connected to the imine function. This provides an asymmetric center in complex **7** because of the differentiation of the two pyridines by the coordination of one. The molecule crystallizes in the centrosymmetric space group $P2_1/n$, and both enantiomers are present in the crystal structure.

Other crystals **8** were obtained from the mother liquor of $[tpip]_2[Co^{II}Cl_4]$ (**6**) and revealed a totally different structure. The complex $[Co^{II}_2(dpmm)_2Cl_4]$ (**8**) (dpmm = di(2-pyridyl)-methoxymethanol), the crystal structure of which is depicted in Scheme 4, belongs to the second category of compounds obtained with tpip. With $CoCl_2$ as the starting material, the degradation of tpip went further than for complex **7**, resulting in the crystallization of the cobalt complex **8**, which contains only fragments of the starting ligand (ligand **G** of Scheme 5 in the Discussion section). Selected bond lengths and angles of complex **8** are given in Table 6.

Table 5. Selected bond lengths [Å] and angles [°] for $[Fe^{II}(dpmmdpi)Cl_2]$ (**7**).

Fe(1)–N(1)	2.133(5)	Fe(1)–Cl(2)	2.325(2)
Fe(1)–N(3)	2.133(5)	C(6)–N(5)	1.306(8)
Fe(1)–N(5)	2.147(4)	C(17)–N(5)	1.479(8)
Fe(1)–Cl(1)	2.307(2)	N(3)–N(4)	3.93
N(1)-Fe(1)-N(3)	146.3(2)	N(5)-Fe(1)-Cl(1)	109.22(14)
N(1)-Fe(1)-N(5)	74.89(19)	N(1)-Fe(1)-Cl(2)	97.13(14)
N(3)-Fe(1)-N(5)	74.53(19)	N(3)-Fe(1)-Cl(2)	99.37(15)
N(1)-Fe(1)-Cl(1)	99.80(14)	N(5)-Fe(1)-Cl(2)	144.19(15)
N(3)-Fe(1)-Cl(1)	103.31(15)	Cl(1)-Fe(1)-Cl(2)	106.53(8)
Fe(1)-N(1)-C(5)	116.7(4)	Fe(1)-N(3)-C(16)	119.7(4)
N(1)-C(5)-C(6)	114.7(5)	N(3)-C(16)-C(17)	118.2(5)
C(5)-C(6)-N(5)	115.4(5)	C(16)-C(17)-N(5)	106.1(5)
C(6)-N(5)-Fe(1)	117.6(4)	C(17)-N(5)-Fe(1)	120.3(4)

Table 6. Selected bond lengths [Å] and angles [°] for $[Co^{II}_2(dpmm)_2Cl_4]$ (**8**).

Co(1)–N(1)	2.119(3)	Co(1)–O(1)	2.380(3)
Co(1)–N(2)	2.124(3)	Co(1)–Cl(2)	2.416(1)
Co(1)–Cl(1)	2.3626(13)	Co(1)–Cl(3)	2.438(1)
Co(1)···Co(1A)	3.574		
N(1)-Co(1)-N(2)	87.47(13)	O(1)-Co(1)-Cl(2)	87.92(9)
N(1)-Co(1)-Cl(1)	95.07(9)	N(1)-Co(1)-Cl(3)	89.53(10)
N(2)-Co(1)-Cl(1)	93.63(9)	N(2)-Co(1)-Cl(3)	172.27(9)
N(1)-Co(1)-O(1)	73.11(11)	Cl(1)-Co(1)-Cl(3)	93.74(3)
N(2)-Co(1)-O(1)	70.39(11)	O(1)-Co(1)-Cl(3)	101.91(7)
Cl(1)-Co(1)-O(1)	160.12(7)	Cl(2)-Co(1)-Cl(3)	85.14(4)
N(1)-Co(1)-Cl(2)	158.80(9)	Co(1A)-Cl(2)-Co(1)	95.44(6)
N(2)-Co(1)-Cl(2)	95.12(9)	Co(1A)-Cl(3)-Co(1)	94.27(6)
Cl(1)-Co(1)-Cl(2)	105.72(13)		

The structure analysis of complex **8** shows a neutral dimeric (di-μ-chloro)dicobalt(II) core. The two metal centers are arranged in a very distorted octahedral geometry. The cobalt(II) ions are coordinated to two nitrogen donor atoms and one oxygen atom of the methoxy group from the dpmm ligand, and one terminal and two bridging chloride anions. The square plane includes the two pyridines with a mean bond length of 2.122 Å, and the two bridging chlorides with significantly longer bond lengths (Co1–Cl2: 2.416(1) and Co1–Cl3: 2.438(1) Å). The latter are especially long com-

0947-6539/99/0506-1770 $ 17.50+.50/0 *Chem. Eur. J.* **1999**, *5*, No. 6

pared to the axial Co–Cl1 bond length of 2.362(1) Å. The coordination sphere is completed by the axial methanolate oxygen of the methoxy group, with a Co1–O1 bond length of 2.380(3) Å, the two coordinated oxygen atoms of both dpmm ligands being located *trans* to each other. The Co···Co distance is 3.574 Å, and the deviation of the cobalt(II) ion from the least-squares plane defined by N1, N2, Cl2, and Cl3 is 0.28 Å.

Discussion

All structures of the complexes obtained with bdpma and manganese, iron, or cobalt salts can be rationalized by metal-catalyzed oxidative degradation of the bdpma ligand as shown in Scheme 5 (when they did not contain the intact bdpma). In the absence of transition metal ions bdpma is highly stable, even in solution, and has been fully characterized.[8]

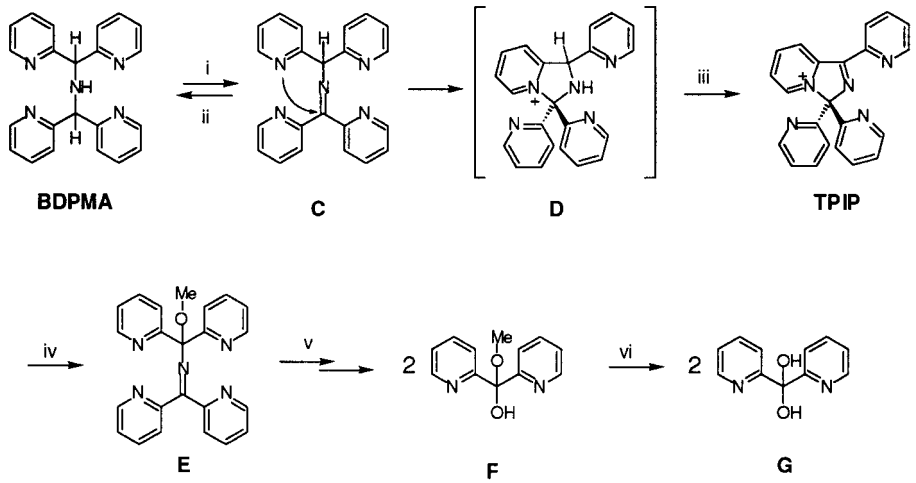

Scheme 5. Proposed degradation mechanism of the polypyridine ligand bdpma via the cationic compound tpip to di(2-pyridyl)ketone hydrate. i) $Fe(NO_3)_3$; ii) Zn, AcOH; iii) MnO_2 or O_2; iv) MeOH, $FeCl_2$ or $CoCl_2$; v) $CoCl_2$; vi) $[Co(OAc)_2]$.

In contrast, in the presence of iron or cobalt salts, several degradation products of bdpma were observed, involving the imine **C** as primary oxidation intermediate. Thereby, two electrons and two protons are abstracted and the metal is reduced from the +3 to the +2 oxidation state.[18] The coordination of the polypyridine ligands certainly facilitates the redox reaction at the metal center by an inner-sphere electron transfer. The imine **C** can be activated by protonation[19] and can then be attacked by a pyridine nitrogen acting as an internal nucleophile to produce a five-membered ring (Scheme 5). Hydrolysis of the imine to the amine **A** and the ketone **B**, the back-reaction of the bdpma synthesis (cf. Scheme 1), should be possible but was not observed in the present case. Cyclization is already known for pyridyl-substituted imines, which are further oxidized to imidazo[1,5-*a*]pyridines after ring closure.[20] This was not possible in the present case because a quaternary carbon was created during the cyclization (labeled C1 in Scheme 3). Consequently, only one C–N double bond could be obtained by dehydrogenation of the five-membered ring (step iii, Scheme 5), and the pyridinium nitrogen remained positively charged. Traces of tpip were previously observed in ^{1}H NMR spectra of imine **C**, suggesting that the oxidation of compound **D** to tpip (step iii, Scheme 5) was also possible with molecular oxygen. To prove that imine **C** was a potential intermediate in the degradation of bdpma to tpip, we decided to prepare tpip from **C**. After preparation of **C** according to literature[8] and subsequent oxidation by MnO_2, tpip was obtained in 73% yield. This showed unambiguously that **C** was an intermediate in the transformation of bdpma to tpip and that the cyclization occurred in high yield. In order to purify tpip, the crude reaction mixture was dissolved in methanol and exposed to a methyl *tert*-butyl ether atmosphere. After one day, crystallization was complete and very clean tpip crystals were collected. tpip is stable in methanol solution and no nucleophilic addition of methanol could be observed; this point will be important in the discussion later.

To understand the further degradation products of bdpma, tpip was employed as a potential ligand instead of bdpma. However, first attempts with $MnCl_2$, $FeCl_3$, and $CoCl_2$ were unsuccessful: tpip remained uncoordinated and counterion exchange was observed. The nitrate counterion of tpip exchanged with the chlorides of $FeCl_3$ and the liberated chloride ions reacted with excess $FeCl_3$ to generate the stable tetrachloroferrate $[Fe^{III}Cl_4]^-$ anion, which was not able to undergo coordination by tpip. Probably, the thermodynamic stability of $[Mn^{II}Cl_4]^{2-}$, $[Fe^{III}Cl_4]^-$, and $[Co^{II}Cl_4]^{2-}$ was the driving force for the simple ion exchange and crystallization of tpip with the anionic metallate complexes as counterion.

In contrast to these results, we did obtain a complex with tpip when using $FeCl_2$. However, the tpip was not intact; a methanol molecule attacked the imidazolium ring and opened it by cleaving the C–N^+ bond of the pyridinium ring. This addition is certainly metal-assisted, since tpip is stable in methanol solution, as already mentioned in the description of the purification procedure or as demonstrated by the crystal structures of $[M^{II}Cl_4][tpip]_2$ and $[Fe^{III}Cl_4][tpip]$, which were crystallized from methanol solutions. The first step should thus be coordination of $FeCl_2$ to two pyridyl moieties connected to the imidazopyridinium unit in the 1 and 3 positions (see tpip numbering used for the NMR spectra, and the imidazole nitrogen (structure **H**, Scheme 6). In consequence, owing to the Lewis acidity of the metal center, the LUMO level of the ring system was lowered, making it more electrophilic and reactive with respect to nucleophilic attack

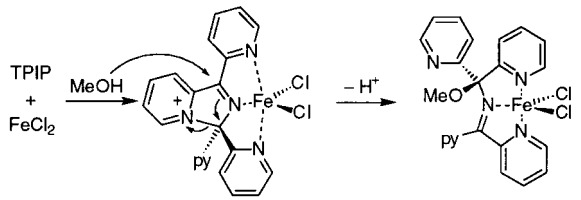

H 7

Scheme 6. Metal-assisted opening of the imidazolium ring of tpip to generate complex **7**.

by a methanol molecule. Furthermore, the coordination of the three nitrogens of tpip introduced a constraint into the molecule which pinched the two coordinated pyridine rings and lengthened the C–N$^+$ bond. The distance between N3 and N4 in the Fe complex **7** was 3.93 Å (Table 5), but in the relaxed tpip molecule the corresponding distance was around 1 Å longer (4.95 Å taken from the distance between C9 and C14 of a tpip salt in Scheme 4). The Lewis acidity and the pinching effect synergetically assisted the methanol addition and the cleavage of the C–N$^+$ bond of the imidazolium ring. Consequently, a non-alkylated pyridine was obtained. With bdpma as ligand, we obtained only a complex with an iron(III) ion, even starting from an iron(II) salt. The most interesting feature of complex **7** was the stabilization of the +2 oxidation state of the iron center by the modified tpip ligand. In contrast, the cobalt analogue of **7** probably exists but was not stable enough to be fully characterized by X-ray analysis. The corresponding red crystals were too small to be correctly analyzed, but the cell parameters were similar to that of the iron complex **7**. From the mother liquor, violet crystals were isolated and analyzed by X-ray studies (complex **8**, Scheme 4). This compound is a further modified tpip ligand corresponding to a hemiacetal of dipyridyl ketone with a methanol molecule (see ligand **F** in Scheme 5).

Conclusion

While attempting to prepare different complexes with the tetrapyridyl ligand bdpma and manganese, iron, and cobalt salts, we were able to trap different degradation products of the bdpma ligand. By identification and preparation of the intermediate product tpip, we showed that the benzylic C–H bonds in the α-position to a heteroatom are the weak point of this polypyridine ligand. This detailed work on polypyridine ligand degradation will be useful in the development of more robust nonheme ligands based on polypyridine units. Such work is in progress in our group.

Experimental Section

General: Commercially available reagents and all solvents were purchased from standard chemical suppliers and used without further purification. Bis[di(2-pyridyl)methyl]amine (bdpma) and di(2-pyridyl)methyl amine were synthesized according to literature procedures.[8] ^{1}H NMR spectra were recorded on a Bruker AM 250 (250 MHz) spectrometer with $CDCl_3$ as solvent; $\delta_H = 7.26$. Elemental analyses were carried out by the Service de Microanalyse du Laboratoire de Chimie de Coordination and all elemental analyses were consistent with the proposed formulas. Mass spectrometry analyses were performed on a Nermag R1010 apparatus (FAB$^+$/*meta*-nitrobenzyl alcohol (MNBA) in DMSO) or on a Perkin–Elmer SCIEX Api 100 spectrometer (ES in MeOH) by the Service de Spectrométrie de Masse de Chimie UPS-CNRS de Toulouse. UV-visible spectra were obtained on a Hewlett-Packard 8452A diode array spectrophotometer, with cuvettes of 1 cm pathlength. IR spectra were recorded on a Perkin–Elmer 983 spectrophotometer. Samples were run as KBr pellets or CH_2Cl_2 solutions. EPR spectra were recorded on a Bruker ESP 300 in X-Band, with an ER035 M gaussmeter (NMR probe) and a EIP 548 hyperfrequency-meter. Powdered samples were loaded in 3 mm cylindrical quartz tubes. Mössbauer measurements were obtained on a constant-acceleration conventional spectrometer with a 25 mCi source of ^{57}Co (Rh-matrix). Magnetic susceptibilities were determined by the Faraday method at room temperature, with a $HgCo(SCN)_4$ matrix ($c/g = 16.44 \cdot 10^{-6}$ emu cgs). Variable-temperature magnetic susceptibility data were obtained with a Quantum Design MPMS Squid susceptometer. The diamagnetism of the ligands was corrected using Pascal's constants. EPR, magnetism and Mössbauer data were recorded by the Service de Mesures Magnétiques du Laboratoire de Chimie de Coordination.

X-ray measurements of 1–8: Crystal data for all structures are presented in Table 7. All data were collected at low temperatures from an oil-coated shock-cooled crystal[21] on a Stoe-IPDS with $Mo_{K\alpha}$ ($\lambda = 0.71073$ Å) radiation. The structures were solved by direct methods by means of SHELXS-97[22] and refined with all data on F^2 by means of SHELXL-97.[23] All non-hydrogen atoms were refined anisotropically. The hydrogen atoms of the molecules were geometrically idealized and refined using a riding model. Refinement of an inversion twin parameter[24] [$x = -0.02(4)$; $x = 0$ for the correct absolute structure and +1 for the inverted structure] confirmed the absolute structure of **2**. Selected bond lengths and angles of **1–8** can be found in Tables 1–6. Crystallographic data (excluding structure factors) for the structures reported in this paper have been deposited with the Cambridge Crystallographic Data Centre as supplementary publication nos. CCDC-108596–108603 (**1–8**). Copies of the data can be obtained free of charge on application to CCDC, 12 Union Road, Cambridge CB2 1EZ (UK) (fax: (+44) 1223-336-033; e-mail: deposit@ccdc.cam.ac.uk).

1,3,3-Tris(2-pyridyl)-3*H*-imidazo[1,5-*a*]pyridin-4-ium (tpip), nitrate form: Di(2-pyridyl)ketone (3.72 g, 20.0 mmol) and di(2-pyridyl)methylamine (3.71 g, 20.0 mmol) were dissolved in absolute isopropanol (120 mL) and dried over 3 Å molecular sieves for 1 h at room temperature. Glacial acetic acid (4.3 mL, 75.0 mmol) was added under N_2 atmosphere and the reaction mixture refluxed for 5 h. MnO_2 (17.40 g, 200 mmol) was then added (the oil bath was removed for the addition). After 1 h heating was switched off and the reaction mixture allowed to cool slowly. After 16 h, solids were removed by filtration. The solvent was evaporated (50 °C, 30 Torr) and the residue dissolved in CH_2Cl_2 (100 mL) and washed with brine (2×30 mL). The crude reaction mixture was purified by column chromatography (SiO_2, MeOH with 2 vol% of HNO_3—this acid provides the counterion for the tpip cation). The resulting brown oil was dissolved in MeOH and exposed to a methyl *tert*-butyl ether atmosphere. 6.02 g (14.6 mmol, 73%) of yellow crystals were obtained. ^{1}H NMR (300 MHz, $CDCl_3$, 25 °C): $\delta = 7.38$ (ddd, $^3J(H,H) = 7.5$ Hz, $^4J(H,H) = 4.8$ Hz, $^5J(H,H) = 0.9$ Hz, 2H, 18-H), 7.60 (ddd, $^3J(H,H) = 7.6$ Hz, $^4J(H,H) = 4.8$ Hz, $^5J(H,H) = 0.9$ Hz, 1H, 12-H), 7.72 (d, $^3J(H,H) = 7.9$ Hz, 2H, 20-H), 7.85 (td, $^3J(H,H) = 7.8$ Hz, $^4J(H,H) = 1.7$ Hz, 2H, 19-H), 8.01 (td, $^3J(H,H) = 7.8$ Hz, $^4J(H,H) = 1.7$ Hz, 1H, 13-H), 8.55 (m, 4H, 6-H, 17-H, 14-H), 8.84 (dq, $^3J(H,H) = 4.9$ Hz, $J(H,H) = 0.8$ Hz, 1H, 11-H), 9.05 (t, $^3J(H,H) = 7.7$ Hz, 1H, 7-H), 9.64 (d, $^3J(H,H) = 8,0$ Hz, 1H, 8-H), 10.08 (d, $^3J(H,H) = 6.0$ Hz, 1H, 5-H); ^{13}C NMR (75 MHz, $CDCl_3$, 25 °C): $\delta = 105.1$ (s, C-3), 124.8 (d, 2C, C-20), 125.2 (d, C-14), 126.1 (d, 2C, C-18), 127.8 (d, C-8), 128.1 (d, C-6), 128.3 (d, C-12), 138.5 (d, C-13), 139.1 (d, 2C, C-19), 145.5 (s, C-8a), 146.2 (d, C-5), 149.4 (d, C-7), 149.6 (s, C-9), 150.7 (d, C-11), 150.8 (d, 2C, C-17), 153.3 (s, 2C, C-15), 162.5 (s, C-1). The structure of [tpip](NO_3) was determined by X-ray crystallography (see text, Scheme 3, and Tables 3 and 7).

Dichloro{bis[di(2-pyridyl)methyl]amine}manganese(II) ([Mn^{II}(bdpma)-Cl$_2$], 1): bdpma (50 mg, 1.41×10^{-4} mol) and $MnCl_2 \cdot 4H_2O$ (26 mg, 1.30×10^{-4} mol) were dissolved separately in MeOH (total volume of 3 mL). The resulting solution was stirred for 15 min and then allowed to stand in a diethyl ether bath for one week. After washing with diethyl ether and drying under vacuum, the solution yielded 10 mg (15%) of colorless

0947-6539/99/0506-1772 $ 17.50+.50/0 *Chem. Eur. J.* **1999**, *5*, No. 6

Table 7. Crystal structure data for compounds **1** to **8**.

	1	**2**	**3**	**4**	**5**	**6**	**7**	**8**
formula	$C_{22}H_{19}Cl_2MnN_5$	$C_{22}H_{19}Cl_2FeN_5O_{0.5}$-$(CH_3OH)_{0.75}$	$C_{26}H_{29}CoN_4O_7$	$C_{22}H_{16}Cl_2Mn_{0.5}N_5$	$C_{22}H_{16}Cl_4FeN_5$	$C_{22}H_{16}Cl_2Co_{0.5}N_5$	$C_{23}H_{19}Cl_2FeN_5O$	$C_{12}H_{12}Cl_2CoN_2O_2$
M_r	479.26	511.95	568.46	448.77	548.05	450.76	508.18	346.07
T [K]	173(2)	173(2)	193(2)	173(2)	193(2)	173(2)	173(2)	173(2)
crystal system	monoclinic	tetragonal	monoclinic	monoclinic	triclinic	monoclinic	monoclinic	monoclinic
space group	$P2_1/n$	$P4_32_12$	$P2_1/c$	$I2/a$	$P\bar{1}$	$I2/a$	$P2_1/n$	$C2/c$
a [Å]	11.145(2)	13.079(1)	11.603(2)	14.626(4)	8.343(1)	14.600(2)	8.237(1)	14.273(3)
b [Å]	16.462(2)	13.079(1)	7.990(1)	14.511(3)	10.249(2)	14.404(2)	17.347(2)	15.937(2)
c [Å]	12.041(2)	27.921(4)	15.186(2)	19.709(7)	14.394(2)	19.818(2)	15.388(1)	13.364(3)
α [°]	90	90	90	90	82.74(2)	90	90	90
β [°]	90.30(2)	90	96.40(2)	103.40(4)	78.62(2)	102.85(1)	90.17(1)	112.17(2)
γ [°]	90	90	90	90	86.99(2)	90	90	90
V [Å^3]	2202.9(6)	4776.2(9)	1399.1(4)	4069(2)	1196.4(3)	4063.3(9)	2198.7(4)	2815.1(9)
Z	4	8	2	8	2	8	4	8
ρ_{calcd} [Mg m^{-3}]	1.445	1.424	1.349	1.465	1.521	1.474	1.535	1.633
$F(000)$	980	2106	592	1836	554	1844	1040	1400
cryst. size [mm]	$0.6\times0.5\times0.1$	$0.7\times0.5\times0.2$	$0.7\times0.1\times0.1$	$0.5\times0.4\times0.1$	$0.5\times0.4\times0.1$	$0.5\times0.4\times0.1$	$0.4\times0.4\times0.1$	$0.7\times0.4\times0.3$
$2\theta_{max}$ [°]	46	46	46	45	46	46	45	46
refl. collected	17908	38511	11343	8006	8809	16457	14520	11312
indep. refl.	3028	3214	1991	2632	3229	2916	2857	2014
R_{int}	0.0539	0.0970	0.0393	0.1427	0.0356	0.0748	0.1099	0.0672
absorption correct.	numerical	numerical	numerical	none	none	numerical	numerical	numerical
T_{min}, T_{max}	0.6803, 0.8631	0.7744, 0.8985	0.8541, 0.9505	–	–	0.7038, 0.8779	0.7807, 0.8934	0.6200, 0.8088
parameters	281	319	237	268	335	267	290	178
R ($I>2\sigma(I)$)	0.0300	0.0549	0.0482	0.0610	0.0489	0.0326	0.0502	0.0362
$wR2$[a] (all data)	0.0669	0.1381	0.1299	0.1668	0.1377	0.0687	0.1296	0.0927
$(\Delta/\rho)_{min}$ [e Å^{-3}]	−0.341	−0.502	−0.390	−0.540	−0.467	−0.480	−0.452	−0.642
$(\Delta/\rho)_{max}$ [e Å^{-3}]	0.249	0.703	0.677	0.379	0.805	0.241	0.423	0.353

[a] $wR2=\{[\Sigma w(F_c^2-F_o^2)^2]/[\Sigma w(F_o^2)^2]\}^{1/2}$.

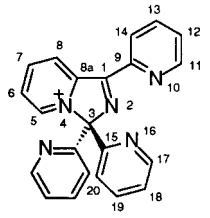

TPIP numbering used for NMR spectra

crystals **1**. FAB-MS: m/z (%) = 443 (100) $[Mn^{II}(bdpma)Cl]^+$; UV/Vis (MeOH): λ_{max} ($\varepsilon\times10^{-3}$ M^{-1}cm^{-1}) = 264 nm (9.2), 318 (3.9). The structure of **1** was determined by X-ray crystallography (see text, Scheme 2, and Tables 1 and 7).

Dichloro-μ-oxo{bis{bis[di(2-pyridyl)methyl]amine}}diiron(III) dichloride ($[Fe^{III}_2(bdpma)_2(O)Cl_2]Cl_2$, 2): By the double-ended needle technique, $FeCl_2\cdot4H_2O$ (195 mg, 9.79×10^{-4} mol) in degassed MeOH (2 mL) was added under nitrogen to a solution of bdpma (346 mg, 9.79×10^{-4} mol) in degassed MeOH (2 mL). The resulting solution was stirred for 15 min under nitrogen and then allowed to stand in a degassed methyl *tert*-butyl ether atmosphere for 3 d. Red crystals of **2** were washed with methyl *tert*-butyl ether and dried under vacuum. The iron centers were probably oxidized by diffusion of molecular oxygen during this 3-day work-up. The yield was 246 mg (48%). ES-MS: m/z = 940.91 $[Fe^{III}_2(bdpma)_2(O)(Cl^-)_3]^+$, 904.45 $[Fe^{III}_2(bdpma)_2(O)(Cl^-)_3-HCl]^+$; UV/Vis (MeOH): λ_{max} ($\varepsilon\times10^{-3}$ M^{-1}cm^{-1}) = 244 nm (15.4), 260 (18.1), 320 (11.2). The structure of **2** was determined by X-ray crystallography (see text, Scheme 2, and Tables 2 and 7).

{Bis[di(2-pyridyl)ketonehydrate}cobalt(III) methanolate ($\{[Co^{III}(dpkH)_2](MeO)(MeOH)\}$, 3): An ethanolic solution (2 mL) of $Co(OAc)_2\cdot4H_2O$ (71 mg, 2.83×10^{-4} mol) was added to a solution of bdpma (100 mg, 2.83×10^{-4} mol) in CH_3CN (2 mL). The resulting dark blue solution was stirred for 5 d at room temperature and then allowed to stand in an ethyl acetate bath. 51 mg (37%) of red crystals of **3** were collected and dried under vacuum after two months. FAB-MS: m/z (%) = 461 (100) $[Co^{III}(dpkH)_2]^+$, 444 (16) $[Co^{II}(dpkH)(dpk)]^+$ (dpk: di(2-pyridyl)ketone), 427 (4) $[Co^{I}(dpk)_2]^+$; ^{1}H NMR (250 MHz, [D$_6$]DMSO, 25 °C): δ = 7.58 (dd, 2H), 7.98 (d, 2H), 8.20 (t, 2H), 8.33 (d, 2H) (further analysis by two-dimensional ^{1}H NMR or ^{13}C NMR was impossible because the complex decomposed in solution after minutes). The structure of **3** was determined by X-ray crystallography (see text, Scheme 3, and Tables 4 and 7).

Bis[1,3,3-tris(2-pyridyl)-3*H*-imidazo[1,5-*a*]pyridin-4-ium] tetrachloromanganate ($[tpip]_2[Mn^{II}Cl_4]$, 4): [tpip](NO_3) (50 mg, 1.21×10^{-4} mol) and $MnCl_2\cdot4H_2O$ (30 mg, 1.52×10^{-4} mol) were dissolved separately in MeOH (total volume of 2 mL). The resulting solution was stirred for 15 min and then allowed to stand in a methyl *tert*-butyl ether bath. After two weeks, 15 mg (24%) of pale red-brown crystals of $[tpip]_2[Mn^{II}Cl_4]$ were obtained. FAB-MS: m/z (%) = 350 (100) $[tpip]^+$. The structure of **4** was determined by X-ray crystallography: selected bond lengths and angles are given in Table 3 and X-ray data in Table 7.

1,3,3-Tris(2-pyridyl)-3*H*-imidazo[1,5-*a*]pyridin-4-ium tetrachloroferrate ($[tpip][Fe^{III}Cl_4]$, 5): [tpip](NO_3) (50 mg, 1.21×10^{-4} mol) and $FeCl_3\cdot6H_2O$ (40 mg, 1.48×10^{-4} mol) were dissolved separately in MeOH (total volume of 3 mL). The resulting solution was stirred for 15 min and then allowed to stand in a methyl *tert*-butyl ether bath. After two weeks, 47 mg (71%) of pale brown crystals were obtained. FAB-MS: m/z (%) = 350 (100) $[tpip]^+$. Under anaerobic conditions, the same crystals of [tpip]-$[Fe^{III}Cl_4]$ were obtained when [tpip](NO_3) and the ferrous salt $FeCl_2\cdot4H_2O$ were used in stoichiometric amounts as starting materials (in contrast, complex **7** was obtained when a 2:1 mixture of tpip and $FeCl_2$ was employed). The structure of **5** was determined by X-ray crystallography: selected bond lengths and angles are given in Table 3 and X-ray data in Table 7.

Bis[1,3,3-tris(2-pyridyl)-3*H*-imidazo[1,5-*a*]pyridin-4-ium] tetrachlorocobaltate ($[tpip]_2[Co^{II}Cl_4]$, 6): [tpip](NO_3) (25 mg, 6.1×10^{-5} mol) and $CoCl_2\cdot6H_2O$ (19 mg, 7.5×10^{-5} mol) were dissolved separately in MeOH (total volume of 2 mL). The resulting red solution was stirred for 15 min and then allowed to stand in a methyl *tert*-butyl ether bath. After 3 weeks, a small quantity of dark green crystals of $[tpip]_2[Co^{II}Cl_4]$ (5 mg, yield = 18%) were filtered off and dried under vacuum. FAB-MS: m/z (%) = 350 (100) $[tpip]^+$. The structure of **6** was determined by X-ray crystallography (see text, Scheme 4, and Tables 3 and 7).

Dichloro{*N*-[di(2-pyridyl)methoxymethyl][di(2-pyridyl)imine]}iron(II) ([Fe^{II}(dpmmdpi)Cl_2], 7): By the double-ended needle technique, $FeCl_2 \cdot 4H_2O$ (28 mg, 1.43×10^{-4} mol) in degassed MeOH (2 mL) was added under nitrogen atmosphere to a solution of two equivalents of [tpip](NO_3) (99 mg, 2.85×10^{-4} mol) in degassed MeOH (2 mL). The resulting solution was stirred for 1 h under nitrogen and then allowed to stand under anaerobic conditions in a methyl *tert*-butyl ether atmosphere. After one week, a small quantity of dark blue crystals of **7** (7 mg, yield = 10 %) were filtered off and dried under vacuum. FAB-MS: m/z (%) = 472 (100) [Fe^{II}(dpmmdpi)Cl]$^+$. The structure of **7** was determined by X-ray crystallography (see text, Scheme 4, and Tables 5 and 7).

Dichloro-μ-dichloro{bis[di(2-pyridyl)methoxymethanol]}dicobalt(II) ([Co_2^{II}(dpmm)Cl_4], 8): After two further weeks, an additional crop of violet crystals was obtained from the mother liquor of [tpip]$_2$[$Co^{II}Cl_4$]. These were washed with methyl *tert*-butyl ether and dried under vacuum. 5 mg (24 %) of **8** was obtained. FAB-MS: m/z (%) = 462 (47) [Co^{II}(dpk)$_2$Cl]$^+$, 278 (100) [Co^{II}(dpk)Cl]$^+$. The structure of **8** was determined by X-ray crystallography (see text, Scheme 4, and Tables 6 and 7).

Acknowledgments

We are grateful to the CNRS for financial support, especially M.R. for a postdoctoral fellowship. We are indebted to Dr. Jean-Pierre Costes (LCC-CNRS) for his contribution to the interpretation of the magnetic measurements, and we thank Alain Mari (LCC-CNRS) for magnetic measurements.

[1] L. Que, Jr., R. Y. N. No, *Chem. Rev.* **1996**, *96*, 2607.
[2] W. O. Koch, H.-J. Krüger, *Angew. Chem.* **1995**, *107*, 2928; *Angew. Chem. Int. Ed. Engl.* **1995**, *34*, 2671.
[3] H. G. Jang, D. D. Cox, L. Que, Jr., *J. Am. Chem. Soc.* **1991**, *113*, 9200.
[4] T. Funabiki, T. Yamazaki, A. Fukui, T. Tanaka, S. Yoshida, *Angew. Chem.* **1998**, *110*, 527; *Angew. Chem. Int. Ed.* **1998**, *37*, 513.
[5] A. Sorokin, L. Fraisse, A. Rabion, B. Meunier, *J. Mol. Catal. A* **1997**, *117*, 103.
[6] a) A. Sorokin, J. L. Séris, B. Meunier, *Science* **1995**, *268*, 1163; b) A. Sorokin, S. De Suzzoni-Dezard, D. Poullain, J.-P. Noël, B. Meunier, *J. Am. Chem. Soc.* **1996**, *118*, 7410; c) A. Sorokin, B. Meunier, *Acc. Chem. Res.* **1997**, *30*, 470; d) A. Hadasch, A. Sorokin, A. Rabion, B. Meunier, *New J. Chem.* **1998**, *22*, 45.
[7] a) M. Lubben, A. Meetsma, E. C. Wilkinson, B. L. Feringa, L. Que, Jr., *Angew. Chem.* **1995**, *107*, 1610; *Angew. Chem. Int. Ed. Engl.* **1995**, *34*, 1512; b) G. Roelfes, M. Lubben, S. W. Leppard, E. P. Schudde, R. M. Hermant, R. Hage, E. C. Wilkinson, L. Que, Jr., B. L. Feringa, *J. Mol. Catal. A* **1997**, *117*, 223.
[8] M. Renz, C. Hemmert, B. Meunier, *Eur. J. Org. Chem.* **1998**, 1271.
[9] C. Hemmert, M. Renz, B. Meunier, *J. Mol. Catal. A* **1998**, *137*, 205.
[10] M. Renz, C. Hemmert, B. Donnadieu, B. Meunier, *J. Chem. Soc. Chem. Commun.* **1998**, 1635.
[11] a) A. Hazell, K. B. Jensen, C. J. McKenzie, H. Toftlund, *J. Chem. Soc. Dalton Trans.* **1993**, 3249; b) E. C. Wilkinson, Y. Dong, L. Que, Jr., *J. Am. Chem. Soc.* **1994**, *116*, 8394.
[12] A. Hazell, K. B. Jensen, C. J. McKenzie, H. Toftlund, *Inorg. Chem.* **1994**, *33*, 3127.
[13] S. Yan, D. D. Cox, L. L. Pearce, C. Juarez-Garcia, L. Que, Jr., J. H. Zhang, C. J. O'Connor, *Inorg. Chem.* **1989**, *28*, 2507.
[14] O. Kahn, *Molecular Magnetism*, VCH, New York, **1993**.
[15] C. J. O'Connor, *Prog. Inorg. Chem.* **1982**, *29*, 203.
[16] R. E. Norman, R. C. Holz, S. Ménage, C. J. O'Connor, J. H. Zhang, L. Que, Jr., *Inorg. Chem.* **1990**, *29*, 4629.
[17] S. O. Sommerer, J. D. Baker, W. P. Jensen, A. Hamza, R. A. Jacobson, *Inorg. Chim. Acta* **1993**, *210*, 173.
[18] The further evolution of the Fe^{II} species was not investigated, but a reoxidation with molecular oxygen seemed very likely. Starting from $FeCl_2$, the Fe^{III} dimer **2** was probably obtained as a result of slow diffusion of molecular oxygen (Scheme 2). In the cobalt case, the metal oxidation step should be the first one to generate a reducible Co^{III} species and to enter the Co^{III}/Co^{II} oxidation system. In contrast, for manganese the oxidation of the metal from Mn^{II} to Mn^{III} by molecular oxygen is less favorable, even for a polypyridine complex. Consequently, a stable Mn^{II} complex **1** could be isolated (Scheme 2) and no ligand degradation was detected.
[19] This protonated species may be generated directly from the bdpma ligand by abstraction of 2 electrons and 1 proton. As tpip has been synthesized from the imine, the formula of the neutral form with subsequent protonation is the preferred presentation in Scheme 5.
[20] A. P. Krapcho, J. R. Powell, *Tetrahedron Lett.* **1986**, *27*, 3713.
[21] D. Stalke, *Chem. Soc. Rev.* **1998**, *27*, 171.
[22] G. M. Sheldrick, *Acta Crystallogr. Sect. A.* **1990**, *46*, 467.
[23] G. M. Sheldrick, SHELXL-97, Program for Crystal Structure Refinement, Universität Göttingen, **1997**.
[24] H. D. Flack, *Acta Crystallogr. Sect. A.* **1983**, *39*, 876.

Received: November 20, 1998 [F1454]

  0947-6539/99/0506-1774 $ 17.50+.50/0